A Novel Method for Measuring Hollow Fiber Membrane Permeability in a Gas-Liquid System

LAURA W. LUND,*§ WILLIAM J. FEDERSPIEL,*†‡ FRANK R. WALTERS,* AND BRACK G. HATTLER*†

Designing an effective intravenous membrane oxygenator requires selecting hollow fiber membranes (HFMs) that present minimal resistance to gas exchange over extended periods of time. Microporous fiber membranes, as used in extracorporeal oxygenators, offer a minimal exchange resistance, but one that diminishes with time because of fiber wetting and subsequent serum leakage. Potentially attractive alternatives are composite HFMs, which inhibit fiber wetting and serum leakage by incorporating a true membrane layer within their porous walls. To evaluate composite and other HFMs, the authors developed a simple apparatus and method for measuring HFM permeability in a gas-liquid system under conditions relevant to intravenous oxygenation. The system requires only a small volume of liquid that is mixed with a pitched blade impeller driven by a direct current motor at controlled rates. Mass flux is measured from the gas flow exiting the fibers, eliminating the necessity of measuring any liquid side conditions. The authors measured the CO_2 exchange permeabilities of Mitsubishi MHF 200L composite HFMs, KPF 280E microporous HFMs, and KPF 190 microporous HFMs. The membrane permeabilities to CO_2 were 9.3×10^{-5} ml/cm^2/sec/cmHg for the MHF 200L fiber, 4.7×10^{-4} ml/cm^2/sec/cmHg for the KPF 280E fiber, and 2.8×10^{-4} ml/cm^2/sec/cmHg for the KPF 190 fiber. From these results it is concluded that 1) because of liquid-fiber surface interactions, the permeabilities of the microporous fibers are several orders of magnitude less than would be measured for completely gas filled pores, emphasizing the importance of measuring microporous fiber permeability in a gas-liquid system; and 2) the liquid diffusional boundary layer adjacent to the fibers generated by the pitched blade impeller is unique to each fiber, resulting in different boundary layer characterizations. *ASAIO Journal* 1996;42:M446–M451.

Hollow fiber membranes (HFMs) are the fundamental exchange elements of contemporary intracorporeal artificial lung designs, including intrathoracic devices for semipermanent lung replacement[1,2] and simpler intravenous devices for temporary support of the reversibly failing lung.[3-5] The capacity of such devices to deliver oxygen to and remove carbon dioxide from the blood is characterized by the overall gas exchange permeability, K, which represents the volumetric rate of gas exchange normalized to fiber surface area and unit partial pressure difference driving exchange. The constituents of the overall permeability are the series resistances to gas transfer of the membrane walls and the blood phase flowing over the surface of the fibers. Because of the inherent geometric design constraint imposed on intracorporeal artificial lungs, membrane surface area is limited, so a primary focus of their design and development is to reduce the blood side mass transfer resistance to meet gas exchange requirements. The natural result of a significant reduction in the blood side resistance is to increase the effect of the resistance of the hollow fiber membranes on the overall device gas exchange permeability. Ultimately, as improved mechanisms for blood side boundary layer reduction are developed, the HFM permeability can pose a limit to the overall device permeability.

Although most clinically available extracorporeal gas exchangers also rely on HFMs, their larger surface area and passive blood flow paths render the HFM resistance to overall device permeability negligible with respect to the blood side resistance. Because of the greater potential effect that the HFM permeability has on the gas transfer performance of an intravenous membrane oxygenator, selection of an appropriate fiber is critical. Not only must the fiber permeability be greater than the desired device permeability so as not to limit gas transfer performance, but it must also remain stable for extended periods of time. Microporous walled hollow fiber membranes provide greater diffusional capability than "true" membrane fiber constructions. However, the performance of microporous oxygenators deteriorates after several hours of use because of fiber wetting and subsequent serum leakage through the pores and into the gas flow path.[6] Strategies to resist or block wetting include using fibers with markedly reduced pore size or using a composite fiber consisting of a thin nonporous (true) membrane layered over or sandwiched within a standard microporous wall.[7,8] In both cases, the strategies meant to resist fluid wetting also diminish fiber wall permeability. This is especially true for composite fibers, in which the nonporous polymer layer can represent an appreciable impediment to diffusion.

Perhaps because of less applicability to extracorporeal oxygenation, limited information appears available on the gas permeability of hollow fiber membranes suitable for an intravenous artificial lung. Commercial microporous fiber specifications often include species dependent permeability values determined from measurements made in a gas-gas system (with gas phases on both sides of the fiber wall). These values are not applicable to predicting mass transfer in an environment with gas on one side and liquid on the other, where diffusion is the dominant mode of gas transport. In a

From the *Artificial Lung Program, †Department of Surgery, ‡Department of Chemical Engineering, and the §Bioengineering Program, University of Pittsburgh, Pittsburgh, Pennsylvania.

Reprint requests: Laura W. Lund, University of Pittsburgh, Room 431, Biotechnology Center, 300 Technology Drive, Pittsburgh, PA 15219.

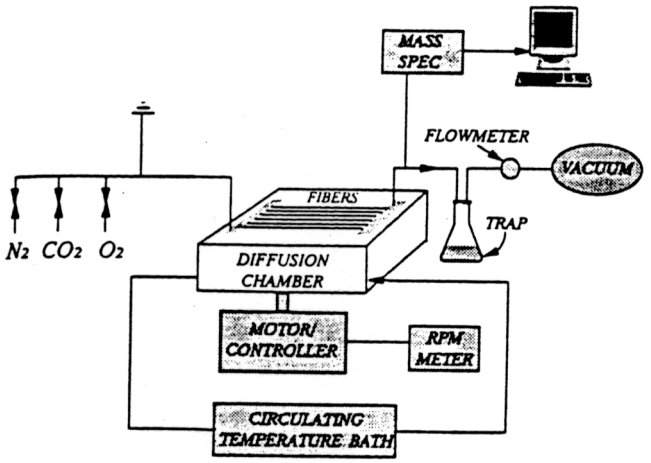

Figure 1. Components used for HFM permeability measurements.

gas-gas system, bulk flow caused by minute pressure differences across the fiber wall also contributes to gas transfer through the membrane, in addition to diffusional flux. Furthermore, even if gas pressures could be maintained at equilibrium across the membrane wall, gas-gas measurements would fail to reflect interactions between the liquid and the surface of the membrane, which might alter permeability.

This article describes a novel method for measuring hollow fiber membrane permeability in a gas-liquid system. A primary feature of the method is the basis of permeability determination using gas-side rather than liquid-side concentration measurements. Not only do gas-side measurements increase the accuracy of the results, but they also simplify the measurement procedure. In addition, determination of system permeability from the time dependent measurement of gas-side species concentrations is independent of the gas flow rate, which simplifies the mathematics and reduces the necessary hardware. Another feature of the method is the small volume of liquid needed to determine fiber permeability. These features enable studies of a variety of fiber types in any liquid of interest, such as blood.

In this article the permeability to CO_2 of three fiber types in water at 37°C is measured using the described apparatus and method. These fibers include Mitsubishi MHF 200L (262 μm outer diameter [OD]) composite fibers, KPF 280E (380 μm OD) microporous fibers, and KPF 190 (244 μm OD) microporous fibers. The results were found to closely compare with those reported previously (Lund *et al.*, 1996) using an earlier version of this apparatus.[9]

Apparatus and Procedure

The principal components of the fiber permeability measurement apparatus are depicted in **Figure 1.** The central component is a diffusion chamber that consists of a parallel arrangement of hollow fiber membranes submerged in a stirred liquid bath of fixed volume (300 ml). Fibers are manifolded in a parallel arrangement to gas flow channels extending from interchangeable lids mounted to the diffusion chamber with screws. The temperature of the liquid bathing the fibers is controlled at 37°C by flowing water from a constant temperature circulating bath (VWR Scientific, Niles, IL) through a small steel tube heat exchanger fixed within the liquid volume. The diffusion chamber also is equipped with compliance balloons for accommodating small liquid volume changes and sealed ports for insertion of a temperature sensor. The mechanism used to stir the liquid recently was upgraded from a 6 cm magnetic stir bar to a quadruple pitched-blade stainless steel impeller, 6 cm in diameter, attached to a shaft that passes through an O-ring bearing at the base of the chamber. The chamber is positioned above and coupled to a 1/8 HP (1,800 rpm) direct current motor (Dayton, Niles, IL) driven by a speed controller (Dart Controls, Zionsville, IN). The upgraded stirring mechanism and drive system were incorporated to improve the flow pattern and to increase the range of stir rates from 50 to 1,500 rpm. With the previously used magnet stirring mechanism, the range of stir rates was limited to 150–500 rpm. The stir rate is measured using an electromagnetic tachometer.

The permeability of the fiber system is determined by a method requiring only gas-side concentration measurements. First, the liquid bath is equilibrated with high concentrations of the test gas of interest, using either 100% O_2 or CO_2 gas drawn under vacuum through the lumen of the fibers. Then, at time zero, the fiber gas source is switched to pure nitrogen to flush the system of test gas, and the change in test gas concentrations (O_2 or CO_2) exiting the fiber bank is continuously measured using a medical gas analyzer (Marquette Electronics, Milwaukee, WI) and recorded on a personal computer with an analog-to-digital board. The rate of the exponential washout of O_2 or CO_2 from the diffusion chamber is determined from these measurements and used to calculate the effective permeability of the fiber-liquid system and to estimate the fiber membrane permeability, as described here.

Calculation of System Permeability

Calculation of the overall system permeability from the gas-side species concentration measurements requires a species mass balance in the liquid phase as follows:

$$\frac{dP_o}{dt} = -\frac{KA}{\alpha V}[P_o(t) - \bar{P}_i(t)] \tag{1}$$

where $\bar{P}_i(t)$ is the average pressure in the fiber at time t, $P_o(t)$ is the partial pressure of mass species (O_2 or CO_2) in the liquid at time t, K is the permeability of the fiber/liquid system, A is the total fiber surface area, V is the volume of liquid in the chamber, and α is the solubility of the mass species in the liquid. Likewise, a mass balance for the same species in the gas phase yields,

$$\frac{d}{dz}[Q\gamma P_i(z,t)] = K\frac{dA}{dz}[P_o(t) - P_i(z,t)] \tag{2}$$

where $\tau = 1/P_{atm}$ and Q is the gas flow rate through the fibers. The solutions to these equations are assumed to be of the form,

$$P_o(t) = P_o' e^{-t/\tau}, \quad \text{and} \quad P_i(z,t) = P_i'(z)e^{-t/\tau} \tag{3}$$

where P_o' is the partial pressure of the mass species in the liquid at t = 0, and $P_i'(z)$ is the partial pressure distribution of

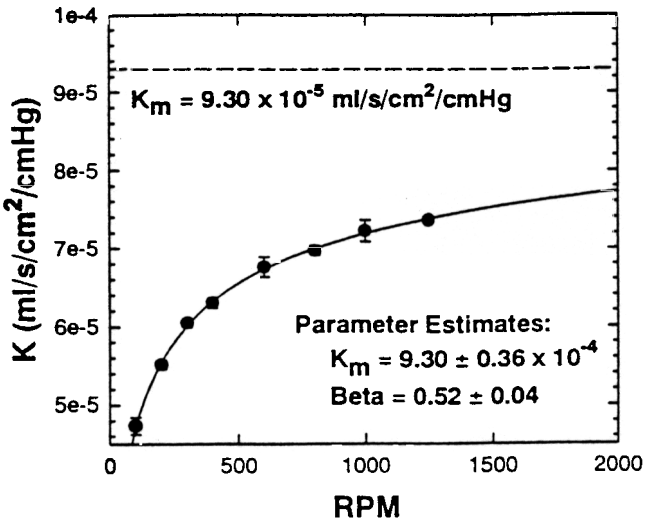

Figure 2. System permeability *vs* stir rate for the MHF 200L composite fibers. The resulting nonlinear regression of equation 10 to these measurements also is shown.

the mass species in the fiber at t = O. Substituting the assumed solutions into the liquid side mass balance into equation 1 yields the following equation for $1/\tau$,

$$\frac{1}{\tau} = \frac{KA}{\alpha V}\left[1 - \frac{\overline{P_i'}}{P_o'}\right] \tag{4}$$

By then substituting the assumed solutions into the gas side mass balance equation, and assuming that the partial pressure of O_2 and CO_2 at the fiber inlet is zero (100% nitrogen), the following expression can be derived for $\overline{P'_i}/P'_e$

$$\frac{\overline{P_i'}}{P_o'} = \frac{e^{-B} + B - 1}{B}, \quad \text{where} \quad B = \frac{KA}{Q_K} \tag{5}$$

If the gas flow rate is low, then $Q_K << KA$ and $B \to \infty$. From equation 5, as $B \to \infty$, $\overline{P_i'}/P_o' = 1 - 1/B$ and thus from equation 4,

$$\frac{1}{\tau} = \frac{KA}{\alpha V}\left[\frac{1}{B}\right] = \frac{Q_K}{\alpha V} \tag{6}$$

i.e., the mass transfer is dependent upon the rate of gas flow through the fibers (flow limited exchange). Conversely, if the gas flow rate is sufficiently high, $KA << Q_K$, and $B \to 0$. From equation 5, $\overline{P_i'}/P_o' \to 0$, and,

$$\frac{1}{\tau} = \frac{KA}{\alpha V'} \tag{7}$$

i.e., mass transfer is dependent upon the fiber-liquid system mass transfer coefficient.

We are interested in isolating the effect of the properties of the fiber membrane on the mass transfer coefficient. Thus, the gas flow rates must be sufficiently high so that gas flux is not flow dependent. However, the gas flow must not be so high as to result in outlet O_2 or CO_2 concentrations that are too low for the accurate determination of the rate at which they diminish. The optimal flow rate can be found experimentally, by comparing values of $1/\tau$ measured at different gas flow rates. A rough estimate of the minimal flow rate at which the gas flux is not flow dependent also can be calculated from these equations.

From the assumed solutions and equation 7, the partial pressure of O_2 or CO_2 measured at the outlet of the fibers is thus governed by the following expression,

$$P(L,t) = P_i'(L)\, e^{-(KA/\alpha V)t}. \tag{8}$$

The mass transfer coefficient, K, can be determined by fitting a line to a plot of the natural log of P(L,t) versus time, where the slope of the line $m = -KA/\alpha V$. Note that the y intercept of this line is $\ln[P_i'(L)]$, which is independent of the slope; thus, it is not necessary to know $P_i'(L)$ (a function of P_o' and $P_i'(O)$) to determine K.

Calculation of Membrane Permeability

The total resistance to mass transfer in the liquid-fiber system is the inverse of the overall system permeability, K. As such, 1/K is determined by the sum of the resistances of the membrane and liquid boundary layers in series:

$$\frac{1}{K} = \frac{1}{K_m} + \frac{1}{K_l}. \tag{9}$$

where K_m and K_l are the respective permeabilities of these phases. A general correlation for the liquid boundary layer permeability would be of the form $K_l = a\hat{}Re^{\beta}Sc^{\gamma}$ where $\hat{a}$, β, and γ are constants, Re is the Reynolds number, and Sc is the Schmidt number. An appropriate characteristic velocity in Re is the ΩL, the product of stir bar rotation rate and length. Thus, for a given fluid and stir bar/diffusion chamber geometry, the liquid boundary layer permeability simplifies to $K_l = a\Omega^{\beta}$, where *a* is also a constant dependent upon fluid, gas species, and geometric parameters. Substituting for K_l equation 9 becomes

$$\frac{1}{K} = \frac{1}{K_m} + \frac{1}{\alpha\Omega^{\beta}} \tag{10}$$

The parameters are determined by plotting K versus Ω and using the Marquardt-Levenberg nonlinear regression algorithm (provided with Sigma Plot Scientific Graphing software, Jandel Scientific, Wilmington, MA) to fit equation 10 to the data.

Results

Figures 2, 3, and 4 show the CO_2 permeability measurements made for the MHF 200L, KPF 280E, and KPF 190 hollow fiber membranes, respectively. The overall gas exchange permeability reflects resistance of the fiber walls and the liquid-side diffusional boundary layers. In the range of mixing studied (from 100 to 1,300 rpm compared with 150 to 500 rpm in previous studies),[9] the resulting liquid-side permeability is sufficiently low so as to have a significant effect on overall system permeability. Accordingly, as stir rate increases, the overall system permeability, K, increases asymptotically toward the limit of the membrane permeability.

Each graph specifies the parameters, K_m and β, estimated from nonlinear regression of equation 10 to the data. The curve fit results are shown plotted through the data. **Figure 5** illustrates a comparison of the estimated fiber permeability

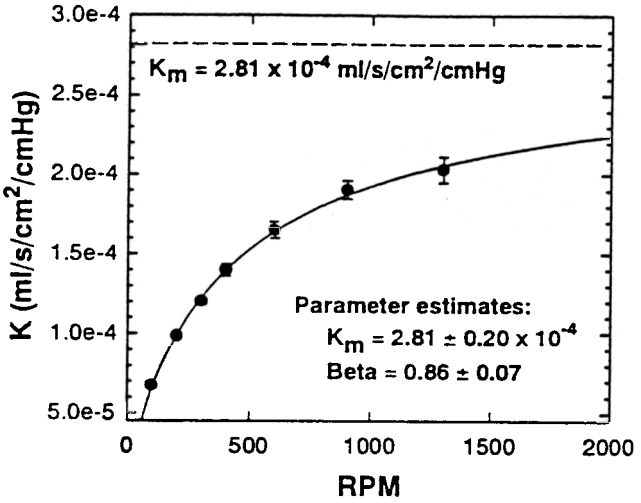

Figure 3. System permeability *vs* stir rate for the KPF 280E microporous fibers. The resulting nonlinear regression of equation 10 to these measurements also is shown.

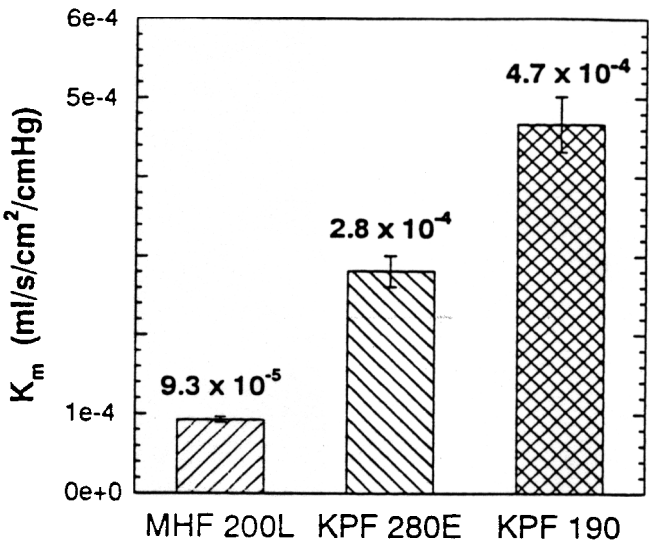

Figure 5. Comparison of estimated CO_2 membrane permeabilities.

for all three fibers. The permeabilities of the MHF 200L, KPF 280E, and KPF 190 fibers were estimated at 9.3×10^{-5}, 2.8×10^{-4}, and 4.7×10^{-4} ml/sec/cm²/cmHg, respectively. In the previous studies performed over a reduced range of stir rate, the CO_2 permeabilities were estimated to be 8.4×10^{-5}, 3.4×10^{-4}, and 3.2×10^{-4} ml/sec/cm²/cmHg, respectively.

Discussion

Determining the membrane permeability from the measured system permeability is based on the ability of the method to effectively separate the contribution of the liquid diffusional boundary layer resistance from that of the membrane resistance. Because of the greater range of stir rates provided with the upgraded system, a more representative

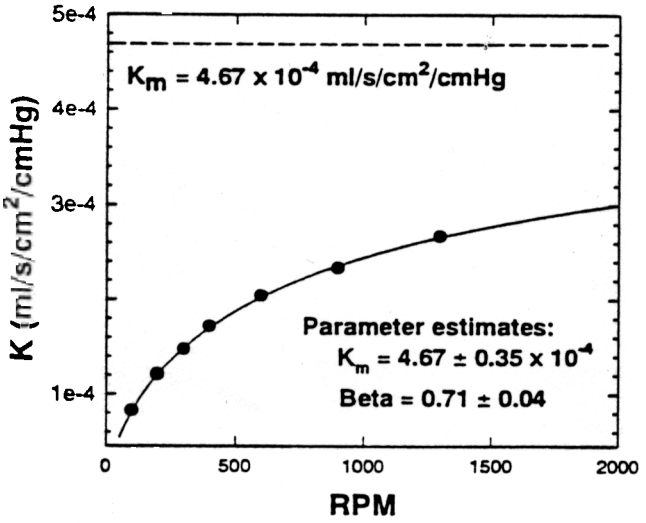

Figure 4. System permeability *vs* stir rate for the KPF 190 microporous fibers. The resulting nonlinear regression of equation 10 to these measurements also is shown.

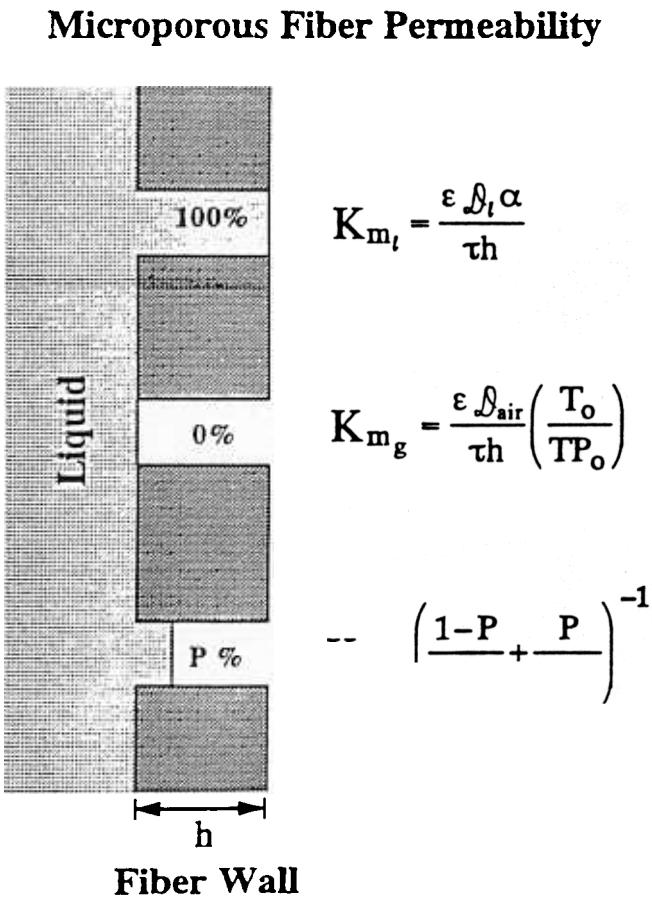

Figure 6. Illustration of the model used to describe the effects of liquid penetration into microporous fiber walls. K_m is fiber permeability, ϵ is porosity, D is diffusivity, α is solubility, τ is tortuosity, h is wall thickness, T is temperature, and P is pressure.

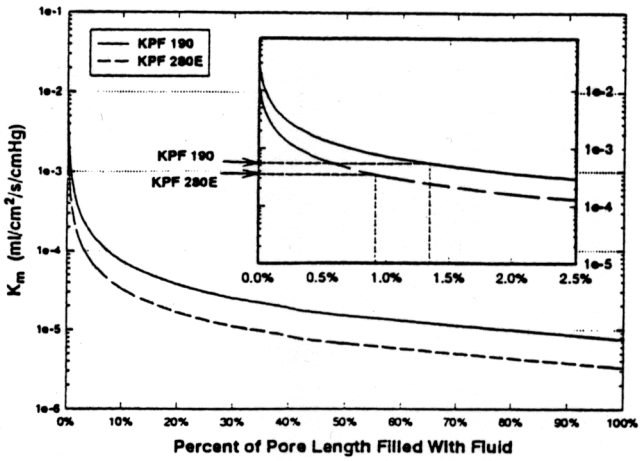

Figure 7. Effect of liquid penetration into the pores of microporous HFMs on the fiber permeability, K_m. The inset scales up the range of 0–2.5% liquid penetration, showing the estimated KPF 280E and 190 permeabilities to be on the order of 1%.

mapping of the liquid boundary layer permeability effect is achieved. In addition, variability of the stir rate at a given set point experienced with the magnetic stirrer was virtually eliminated by the motor and controller, resulting in smaller error bars for the system permeabilities measured at a given stir rate. The estimated CO_2 permeabilities determined using the method described here compare closely with measurements made with the apparatus before the stirring mechanism upgrade.[9] Thus, although comparable with previous measurements, the results obtained with the upgraded system yield greater accuracy in the parameter estimation procedure.

The permeability of the MHF 200L composite HFM to CO_2 was estimated to be 9.3×10^{-5} ml/sec/cm²/cmHg. This fiber is a composite fiber consisting of a 1 μm thick polyurethane solid membrane layer sandwiched within polyethylene microporous layers, with a total wall thickness of 26 μm. The solid membrane layer represents the dominant resistance of the membrane wall to mass transfer. Accordingly, the MHF 200L permeability is smaller than those of the microporous fibers that provide a completely gas filled path for species diffusion. The KPF 280E microporous fiber has a wall thickness of 50 μm, whereas the KPF 190 wall thickness is only 22 μm. The estimated permeabilities of these two fibers reflect this difference. The estimated KPF 280E permeability of 2.8×10^{-4} ml/sec/cm²/cmHg was 40% less than the KPF 190 permeability of 4.7×10^{-4} ml/sec/cm²/cmHg. The porosity and pore sizes of each of these fibers are being examined using scanning electron microscopic study to explore additional possible causes of differences in permeability of these fibers.

The permeabilities of the microporous fibers, although greater than that of the composite fiber (as expected), are less than would be expected if it were assumed that the pores are 100% gas filled. As suggested by Qi and Cussler (1985) in a study of microporous fibers for gas absorption, the presence of liquid within the pores can markedly reduce the gas exchange permeability of a microporous fiber.[10] In our previous work, the effect on fiber permeability of liquid infiltration was modeled and compared with the measurement results.[9] **Figure 6** illustrates the concept of this model and the relationships used to determine fiber permeability for the situations of 100% gas filled, 100% liquid filled, and partial filling of the pores. Assuming 100% gas filled pores, the expected permeability of the KPF 280E and 190 fibers would be 1.3×10^{-2} and 3.0×10^{-2} ml/sec/cm²/cmHg, respectively. Using this same model to evaluate the permeabilities measured with the upgraded system, similar levels of infiltration were found. The estimated CO_2 permeability of the KPF 280E is approximately two orders of magnitude less than that of gas filled pores but surprisingly represents a penetration depth of only 0.9% and, similarly for the KPF 190 fiber, a penetration depth of only 1.3%, as shown in **Figure 7.** Because both fibers were modeled as having the same porosity (45%) and pore size (0.04 μm), the percent of pore length filled with water for the KPF 190 fiber is expected to be greater than that of the KPF 280E fiber because of the relatively thinner wall thickness. We hypothesize that the mechanism of infiltration is related to the protrusion of the liquid-gas surface meniscus into the pores and that the depth of penetration is a function of surface tension, pressure difference between the gas and liquid phases, and fiber material. Because of the significant effect of infiltration on fiber permeability, studies will be conducted using the method described in this article to test this hypothesis.

The mass transfer correlation exponent β, which reflects boundary layer characteristics, is not necessarily the same for each fiber type **(Figures 2–4).** However, the liquid flow patterns generated by the impeller should result in similar boundary layer thicknesses for similar fiber diameters, regardless of the fiber type. The tension of the different fibers when mounted to the lids was not the same, so differences in fiber vibrations within the diffusion chamber resulted. We believe that the resulting differences in flow patterns yield different β values. In addition, differences in surface roughness of the various fibers types may result in the same effect. To confirm this conclusion, fibers will be mounted at different tensions and the resulting permeability estimates compared for positive correlation of variations in β and for consistency in permeabilities.

References

1. Fazzalari FL, Montoya JP, Bonnell MR, Bliss DW, Hirschl RB, Bartlett RH: The development of an implantable artificial lung. *ASAIO J* 40: M728–M731, 1994.
2. Vaslef SN, Cook KE, Leonard RJ, Mockros LF, Anderson RW: Design and evaluation of a new low pressure loss, implantable artificial lung. *ASAIO J* 40: M522–M526, 1994.
3. Mortensen JD, Berry G: Conceptual and design features of a practical, clinically effective intravenous mechanical blood oxygen/carbon dioxide exchange device (Ivox). *Int J Artif Organ* 12(6): 384–389, 1989.
4. Hattler BG, Johnson PC, Sawzik PJ, *et al:* Respiratory dialysis: a new concept in pulmonary support. *ASAIO J* 38: M322–M325, 1992.
5. Snider MT, High KM, Richard RB, *et al:* Small intrapulmonary artery lung prototypes: design, construction, and *in vitro* water testing. *ASAIO J* 40: M735–M739, 1994.
6. La Pierre RA, Howe RJ, Haw MP, Elliott M: Oxygenators for paediatric cardiac surgery, in Jonas RA, Elliott MJ (eds), *Cardiopulmonary Bypass in Neonates, Infants and Young Children,* Boston, Butterworth and Heinemann, 1994, pp. 173–184.

7. Yasuda H, Lamaze CE: Transfer of gas to dissolved oxygen in water via porous and nonporous polymer membranes. *J Appl Polymer Sci* 16: 595–601, 1972.
8. Kamo J, Uchida M, Hirai T, Yasida H, Kanada K, Takemura T: A new multilayered composite hollow fiber membrane for artificial lung. *Artif Organs* 14(5): 369–372, 1990.
9. Lund LW, Federspiel WJ, Hattler BG: Gas permeability of hollow fiber membranes in a quid system. *J Membrane Sci.* [In press.]
10. Qi Z, Cussler EL: Microporous hollow fibers for gas absorption: II. mass transfer across the membrane. *J Membrane Sci* 23: 333–345, 1985.